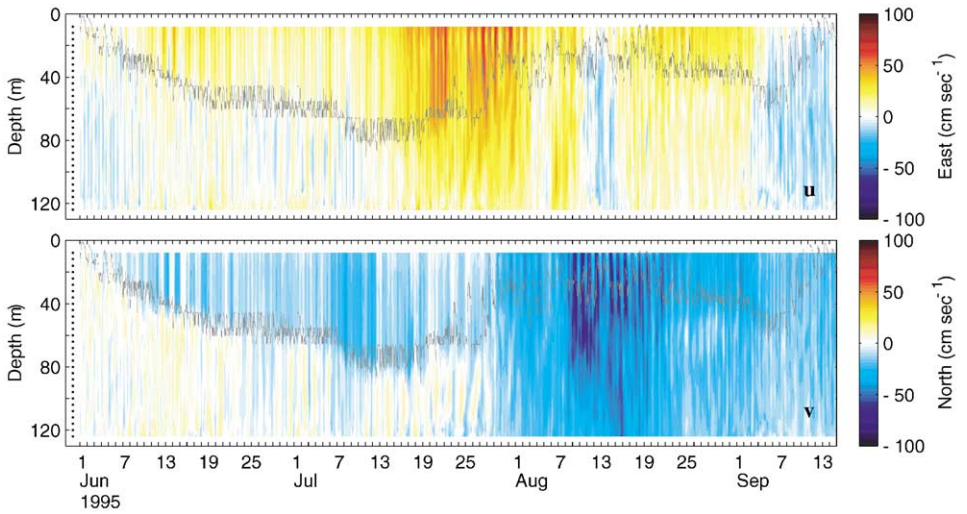

Fig. 23. The east and north components of velocity at SIO-S during the SW Monsoon. The mixed layer depth is shown in gray.

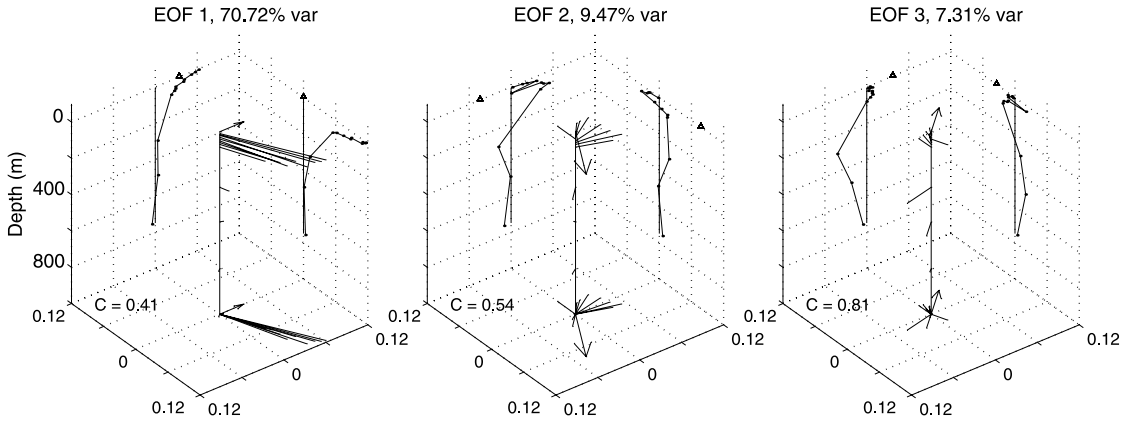

Fig. 24. The first three EOFs of the velocity and scaled wind stress at WHOI during the SW Monsoon. The correlation coefficients, C, between the time-series of the amplitude of each EOF and the wind stress are shown, as is the percentage of the variance that each EOF is associated with. As in Fig. 10, the stick vectors indicate the three-dimensional structure of the velocity EOF, the arrow is the contribution from the variance-scaled wind stress, and the vectors are projected onto the x-, y-, and z-axis planes (triangle for the wind, z-projection at 1000 m depth).

relative to 80 m (Fig. 25b), which remains below the mixed layer, shows that a large proportion of this transport is not confined to the mixed layer, and occurs late in the SW Monsoon when winds are reduced. The strength of the transport in the upper 80 m, both raw and relative to the 80 m velocity (Fig. 25c) is much stronger than the theoretical transport due to the locally driven surface currents.

Satellite altimetry again provides us with a context within which to interpret these observations. At the beginning of the SW Monsoon, the mooring site is in a region of nearly no anomaly from the mean. By the end of June (Fig. 26), there is an eastward jet, well north and west of the mooring, several hundred kilometers off the coast of Oman, and a mild cyclonic feature just north of the mooring site. By the end of July an offshore jet